

# Bifurcation Spiking Neural Network

Shao-Qun Zhang, Zhao-Yu Zhang, Zhi-Hua Zhou

*National Key Laboratory for Novel Software Technology  
Nanjing University, Nanjing 210023, China*

{zhangsq,zhangzhaoyu,zhouzh}@nju.edu.cn

---

## Abstract

Spiking neural networks (SNNs) has attracted much attention due to its great potential of modeling time-dependent signals. The firing rate of spiking neurons is decided by *control rate* which is fixed manually in advance, and thus, whether the firing rate is adequate for modeling actual time series relies on fortune. Though it is demanded to have an adaptive control rate, it is a non-trivial task because the control rate and the connection weights learned during the training process are usually entangled. In this paper, we show that the firing rate is related to the eigenvalue of the spike generation function. Inspired by this insight, by enabling the spike generation function to have adaptable eigenvalues rather than parametric control rates, we develop the *Bifurcation Spiking Neural Network* (BSNN), which has an adaptive firing rate and is insensitive to the setting of control rates. Experiments validate the effectiveness of BSNN on a broad range of tasks, showing that BSNN achieves superior performance to existing SNNs and is robust to the setting of control rates.

*Key words:* Spiking Neural Network, Firing Rate, Control Rate, Eigenvalues, Bifurcation

---

## 1. Introduction

Spiking neural networks (SNNs) take into account the time of spike firing rather than simply relying on the accumulated signal strength in conventional neural networks, and thus offer the possibility for modeling time-dependent data series [GK02, VGT05]. So the firing rate of spiking neurons becomes arguably the most important measure for characterizing the ability of SNNs for modeling time series [BDM13, CCL19]. The firing rate is dominated by many factors, such as neural input, connection weights, and control rates of the spike generation function. And it is sensitive to the setting of these factors, especially the control rate.

In previous works, control rate is usually pre-given and fixed, which results in the learning performance of SNNs is dependent on a careful tuning of this hyper-parameter.

However, achieving an adaptive firing rate with respect to the control rate is a very tricky task since the control rate and connection weights are entangled during the training process. So the approaches of learning hyper-parameters in conventional neural networks cannot be directly used to solve this issue. An alternative way is to sample the control rates from a certain pre-defined distribution and find the optimal ones by alternating optimization. Nevertheless, this method usually succeed depends on an apposite distribution setting, and would result in a larger computation and storage.

In this paper, we propose the *Bifurcation Spiking Neural Network* (BSNN) for achieving adaptive firing rates. We first show that the firing rate of spiking neurons is related to the eigenvalues of spike generation functions. And then by exploiting the bifurcation theory, we convert the issue of parameterizing the control rates into a new problem of learning apposite eigenvalues. So BSNN not only tackles the challenge that control rates interact with connection weights, leading to a robust setting of control rates, but also works with considerable less computation and storage in comparison with the alternating optimization approaches. The experiments conducted on a delayed-memory XOR task and 3 benchmark datasets demonstrate the effectiveness of BSNN, showing that its performance not only surpasses existing SNNs but also robust to the setting of control rates.

The rest of this paper is organized as follows. We first review some preliminary knowledge about spiking neural models in Section 2, and then reveal the close-knit relation of firing rates and eigenvalues of spike generation functions in Section 3. In Section 4, we formally introduce BSNN and present a concrete approach for implementing BSNN with a multi-layer architecture. The experiments are conducted in Section 5. Finally, we conclude our work in Section 6.

## 2. Spiking Neural Model

The *leaky integrate-and-fire* (LIF) neuron is probably one of the simplest spiking generation functions, but it is still very popular due to the ease that it can be analyzed and simulated [HE15]. Here, we review a general form of the LIF equation, which with  $M$ -dimensional input signals  $\mathbf{I}(t) = \{I_1(t), \dots, I_M(t)\}$

and a rest voltage  $u_{rest}$  as follows:

$$\tau \frac{d u_k}{d t} = u_{rest} + \gamma_k \cdot u_k + \sum_{j=1}^M W_{kj} I_j(t), \quad (1)$$

where  $\tau$  is the membrane time constant,  $u_k(t)$  represents the membrane potential of the  $k$ -th neuron at time  $t$ ,  $W_{kj}$  is the corresponding connection weight, and  $\gamma_k$  denotes the control rate with respect to the  $k$ -th neuron, which is usually preset a fixed value  $-1$  according to existing SNNs.

Particularly, the eigenvalue  $\rho_k$  of the  $k$ -th LIF neuron is equal to the quotient of  $\gamma_k$  and  $\tau$  by solving the following algebraic formulation:

$$\frac{d}{dt} \begin{pmatrix} u_1 \\ \vdots \\ u_M \end{pmatrix} = \frac{1}{\tau} \begin{pmatrix} \gamma_1 & & \\ & \ddots & \\ & & \gamma_M \end{pmatrix} \cdot \begin{pmatrix} u_1 \\ \vdots \\ u_M \end{pmatrix}.$$

The supplemental materials about the eigenvalues and the algebraic formulation of an ODE dynamic system can be seen from Appendix.

Based on Spike Response Model (SRM) scheme [Ger95], the LIF equation has a general solution with  $u_{rest} = 0$  as follows:

$$u_k(t) = \sum_{j=1}^M W_{kj} \left[ \int_{t'}^t \exp\left(\gamma_k \frac{s-t'}{\tau}\right) I_j(s) ds \right], \quad (2)$$

where  $t'$  denotes the last firing time  $t' = \max\{s \mid u(s) = u_{firing}, s < t\}$ .

The LIF model mentioned above describes a resistor-capacitor circuit that the spiking neuron can only be activated when the membrane potential  $u(t)$  reaches a certain threshold  $u_{firing}$  (firing threshold). After firing, the neural membrane potential is instantaneously reset to a lower value  $u_{rest}$  (rest voltage). Formally, we can employ a spike excitation function  $f_e$  to formulate this procedure:

$$f_e : u \rightarrow S, \text{ where } S_k(t) \triangleq \left\lfloor \frac{u_k(t)}{u_{firing}} \right\rfloor.$$

## Neural Encoding

In SNNs, input signals are usually pre-converted into a spiking version, that is, encoded by a Poisson distribution or recorded by a Dynamic Vision Sensor (DVS) [QRK<sup>+</sup>05, ANDL18]. Speaking formally, a period of input  $I(0 : T)$  received by an input channel can be regarded as one sampled from a certain Poisson process with an underlying parameter  $\lambda$ , that is,

$$I(0 : T) \sim \pi(\lambda) = \frac{\lambda^K e^{-\lambda} T}{K!}.$$

By exploiting the spike generation function, the input spike train is integrated as

$$\int_{t'}^t \exp\left(\gamma_k \frac{(s - t')\gamma_k}{\tau}\right) I(s) ds$$

in Pre-synapse. Ideally, without the “leaky” term, or equally  $\gamma_k \equiv 0$ , the integrated voltage dynamic in Pre-synapse would obey a standard Poisson process. For a popular setting  $\gamma_k \equiv -1$ , it is obvious that the energy of voltage trains is less than the standard Poisson process. Furthermore, this “leaky” Poisson process can be regarded as an integration of some underlying distribution  $(\lambda^K e^{-1/\tau-\lambda})/K!$ . In other words, leaky integration is equivalent to integrating a “leaky” distribution. For a more general case, it is not hard to infer that the spike generation function with control rate  $\gamma$  is able to convert a regularized Poisson distribution into a reproducing distribution  $(\lambda^K e^{\gamma/\tau-\lambda})/K!$  with the equal expectation and standard deviation  $\lambda e^{\gamma/\tau}$ . And different control rates lead to different temporal reproducing representations. Figure 1(a) gives a vivid illustration for this procedure.

### 3. Firing Rate of Spiking Neurons

The firing rate of spiking neurons is a significant indicator for indicating the representation ability of SNNs. Here, we are going to investigate the roles of firing rates in SNNs by a simple reproducing representation experiment, and then show the importance of eigenvalues on the firing rate.

For simplicity, we take a feed-forward SNN with one input channel, one hidden layer ( $N$  spiking neurons), and one output spiking neuron as an example. For a period of input  $I(0 : T)$ , the spike trains transmitted

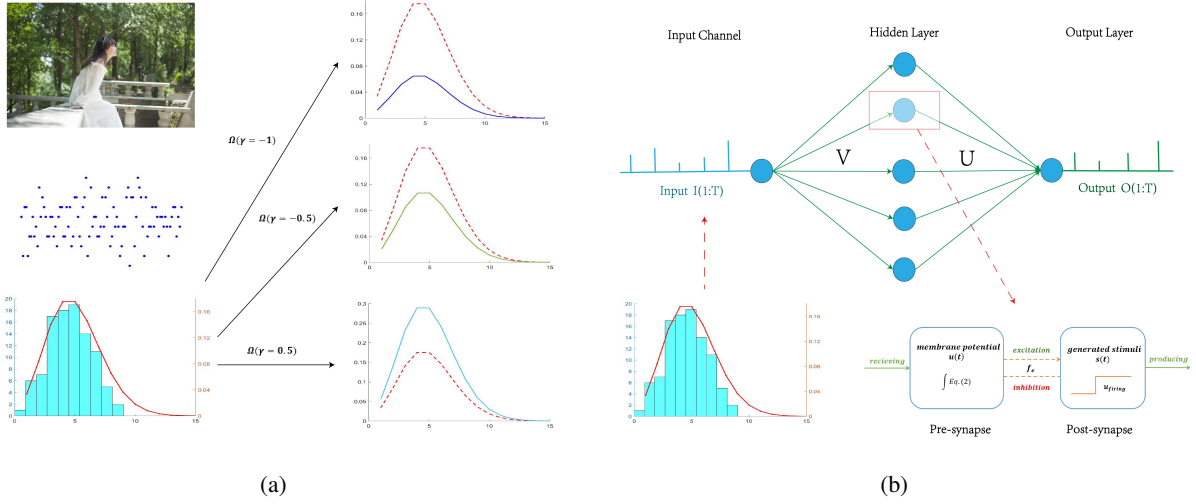


Figure 1: (a) An illustration of the neural encoding in spiking versions. The right three plots display the procedure of the spike coding. The red dashed lines in the left three pictures represent the standard Poisson distribution, while three solid lines indicate the reproducing representation functions, respectively. (b) The feed-forward SNN architecture with one input channel, one hidden layer ( $N$  spiking neurons), and one output.

between layers abide by the following procedure:

$$\begin{cases} O(t) = f_e \left[ \sum_{i=1}^N U_i \int_{t'}^t e^{(s-t')\rho_o} S_i(s) ds \right], \\ S_i(t) = f_e \left[ V_i \int_{t'}^t e^{(s-t')\rho_i} I(s) ds \right], \end{cases}$$

where  $\rho_i$  and  $\rho_o$  indicate the eigenvalue of  $i$ -th hidden spiking neuron and output neuron, respectively.  $U_i$  and  $V_i$  denote the connection weights. Merging the two formulas above and approximating the spike excitation function  $f_e(u_t) \approx \frac{u_t}{u_{firing}}$  (because  $f_e$  will never cause any energy wastage), the total spike count fired from the output neuron during  $(0 : T]$  becomes:

$$C = \frac{1}{u_{firing}^2} \sum_{i=1}^N U_i V_i \left[ \int_0^T e^{(s-t')(\rho_o + \rho_i)} I(s) ds \right].$$

So we can calculate the firing rate according to  $F = C/T$ . Suppose  $I(0 : T)$  are sampled from a Poisson process  $\pi(\lambda_0)$ , then the firing rate obeys a parametric stochastic process with learnable connection weights  $U_i$  and  $V_i$ :

$$F \sim \frac{1}{u_{firing}^2 T} \sum_{i=1}^N U_i V_i \frac{\lambda_0^K T^K}{K!} e^{(\rho_i + \rho_o - \lambda_0)T}. \quad (3)$$

Next, we are going to verify whether the firing rate described in Equation 3 is adaptive, that is, whether the concerned stochastic process led by Equation 3, that has sufficient neurons  $N$ , can approximate any Poisson process in  $(0, T]$ . Let  $\pi(\lambda^*)$  denote the target Poisson process in  $(0, T]$ , then the aforementioned approximation issue is equivalent to solve the following implicit equations:

$$\begin{cases} \sum_{i=1}^N \exp\left(\rho_i + \rho_o - \lambda_0 + \lambda^* + K \ln \frac{\lambda_0}{\lambda^*}\right) = 1, \\ \sum_{i=1}^N U_i V_i \left(\frac{\lambda_0}{\lambda^*}\right)^K = 1. \end{cases} \quad (4)$$

So the issue of achieving adaptive firing rates is converted into a new problem of how to solve these implicit equations. Equation 4 comprises two parts: a quasi-linear equation (the first one) with respect to the eigenvalues and a compound equation (the second one) related to connection weights  $U_i$  and  $V_i$ . Due to the exponential operation, these two equations do not conflict with each other. In neural networks, it is not difficult to solve the compound equation for obtaining a group of apposite connection weights. So next, we are going to discuss the solution of the quasi-linear one.

If we preset all eigenvalues as a uniformly constant as existing SNNs usually do, the firing rate of spiking neurons is non-adaptive, leading to a limited representation ability of SNNs. For example that  $\rho_i \equiv -1$ , the stochastic process

$$\frac{1}{u_{firing}^2} \sum_{i=1}^N U_i V_i \frac{\lambda_0^K T^K}{K!} e^{(-2/\tau - \lambda_0)T}$$

only dependent on learnable connection weights  $U_i$  and  $V_i$  even cannot reproduce the raw input process  $\lambda_0^K T^K \exp(-\lambda_0 T)/K!$ . Furthermore, if we force the eigenvalues of spiking generation functions to be equal, the representation ability of SNNs is still limited according to the rewritten quasi-linear equation:

$$\exp\left(\frac{2\rho}{\tau} - \lambda_0 + \lambda^* + K \ln \frac{\lambda_0}{\lambda^*}\right) = \frac{1}{N},$$

where “2” denotes the number of spiking layers. So the eigenvalues of spike generation functions need to be diverse.

For a more complex case, that is, consider a SNN with  $M$  input channels and  $N$ -dimensional hidden spiking neurons, where each input channel receives a sequence of spikes sampled from  $\pi(\lambda_j)$ ,  $j = 1, \dots, M$ , then

the parametric energy process in Equation 3 becomes:

$$C \sim \frac{1}{u_{firing}^2} \sum_{i=1}^N \sum_{j=1}^M U_i V_{ij} \left\langle \frac{\lambda_j^K T^K}{K!} e^{-\lambda_j T}, e^{(\rho_i + \rho_o)T} \right\rangle. \quad (5)$$

Equation 5 suggests that the parametric eigenvalues  $\rho_i$  leads to a basis function in SNN. So the roles of eigenvalues  $\rho_i$  and learnable connection weights  $U_i$  and  $V_{ij}$  are clearly distinguished. This means the parametric eigenvalues play an important and irreplaceable role in SNNs and cannot be covered by the learnable connection weights.

In summary, eigenvalues of the LIF function indeed have a great and sensitive influence on achieving an adaptive firing rate of SNNs. And the role of eigenvalues cannot be replaced by connection weights. On the contrary, both the ways that presets all eigenvalues to a fixed constant and that employs unified eigenvalues in SNNs would impede the performance of SNNs, leading to whether the firing rate is adequate for modeling actual time series relies on fortune.

### 3.1. Approaches for Parameterizing Control Rates

An intuitive idea for achieving an adaptive firing rate in SNNs is to parameterize the control rates, since the control rate of LIF model is equivalent to its eigenvalue. However, training SNNs with parametric control rates rather than original fixed constant is a brand-new challenge, where the experience of training hyper-parameters in neural networks can hardly be employed. The difficulty is twofold. (1) The existing SNNs are almost trained based on SRM scheme. This leads to the membrane potential in Equation 2 is dominated by the product of connection weights  $W_j$  and control rate  $\gamma_k$ . It is very hard to optimize this problem by simply utilizing gradient-based methods. (2) The roles of control rates and connection weights are distinct during the SNNs training procedure; the control rate is convolved with the received spikes aggregated by connection weights. So the spike errors caused by control rates spread temporally, while connection weights only transmit errors between layers. To sum up, it is a very tricky challenge for conventional approaches to training a SNN with parametric control rates.

An alternative approach to alleviate the issue is to employ alternating optimization for estimating control rate hyper-parameters. The key idea is to regard the control rates is a group hyper-parameters generated from a prior distribution, so that solving for each learnable variable (connection weights or control rates) reduces to well-known methods. In general, we list this optimization procedure as follows:

**Initialization:** Sampling a group of control rates  $\gamma$  from a pre-given distribution, such as the uniform distribution  $\mathcal{U}[-1, 1]$ . Then spikes spread according to:

$$\left\{ \begin{array}{l} S_j^1(t) = I_j(t), \\ u_k^{l+1}(t) = \sum_{j=1}^{n_l} W_{kj}^l \left[ \int_{t'}^t \exp\left(\gamma_k^{l+1} \frac{t' - s}{\tau}\right) S_j^l(s) ds \right], \\ S_k^{l+1}(t) \leftarrow f_e\left(u_k^{l+1}(t)\right). \end{array} \right.$$

**Update connection weights:** How to update the connection weights  $\mathbf{W}$  with fixed  $\gamma$  depends on the choice of error-propagation techniques. Here, we employ a seminal work, SLAYER [SO18] as a basic model.

**Update  $\gamma$ :** We solve  $\arg \min_{\gamma} \text{Loss}(\gamma | \mathbf{I}, \mathbf{Y}; \mathbf{W})$ , where  $\mathbf{Y}$  denotes the supervised signals. Thus, fast algorithm, such as alternating coordinate descent can be applied directly to find a collection of apposite control rates.

Obviously, the approaches based on alternating optimization place larger demands on computation and storage, and usually converge slowly in neural networks.

## 4. Bifurcation Spiking Neural Networks

In this section, we are going to introduce the BSNN for achieving adaptive firing rates of SNNs. The core idea of BSNN is to separate the eigenvalues of spike generation functions from the control rates, with contrast to the LIF mechanism that the eigenvalue of the LIF model is equal to its control rate. (1) By enabling the spike generation function to have adaptable eigenvalues, BSNN can poss an adaptive firing rate. (2) And since the new-born parameters for achieving adaptable eigenvalues are independent of the connection weights, the issue caused by entangled control rates and connection weights is self-defeating. Further experiments demonstrate that the performance of BSNN is insensitive to the setting of control rates.

### 4.1. Basic Bifurcation Neurons

Bifurcation theory is the mathematical study of dynamical systems, a bifurcation occurs when a small smooth change of the parameter values (often the bifurcation hyper-parameters pass through a critical point)



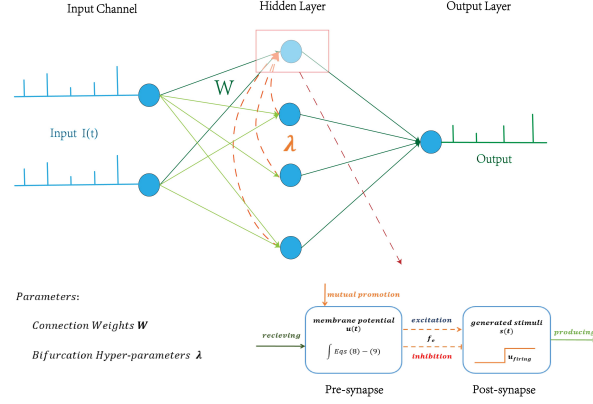


Figure 2: The workflow of neurons in a feed-forward BSNN.

causes a sudden topological change in its behavior [Onu02, Kuz13]. Its central mechanism is to employ the mutual promotion made to other equations of the dynamic system to achieve diverse eigenvalues.

Inspired by this recognition, we propose the bifurcation neurons model:

$$\tau \frac{\partial \mathbf{u}(t)}{\partial t} = \gamma \mathbf{u}(t) + \lambda \mathbf{u}^* + \mathbf{I}(t), \quad (6)$$

where  $\gamma$  is the control rate and  $\lambda$  is the bifurcation hyper-parameters.  $\mathbf{u}^*$  portrays the mutual promotion between neurons, for simplicity, we here denote the mutual promotion of the  $k$ -th neuron as  $u_k^* = \sum_{i \neq k} u_i + o(|u_k|)$ , where  $o(\cdot)$  denotes the high-order term of  $u_k$ , then Equation 6 could be rewritten as:

$$\begin{cases} \tau \frac{\partial u_1(t)}{\partial t} = \gamma u_1(t) + \sum_{i \neq 1} \lambda_{1i} u_i + o(|u_1|) + I_1(t), \\ \vdots \\ \tau \frac{\partial u_n(t)}{\partial t} = \gamma u_n(t) + \sum_{i \neq n} \lambda_{ni} u_i + o(|u_n|) + I_n(t). \end{cases}$$

As we can see, the basic building block of BSNN is a system of equations with respect to a cluster of spiking neurons. Regarding this cluster of spiking neurons as a spiking layer and reusing Equation 6 layer by layer, we can establish a feed-forward multi-layer architecture, as shown in Figure 2.

#### 4.2. Adaptive Firing Rate

To ensure BSNN have an adaptive firing rate, we need to verify whether the stochastic process produced by BSNN is able to approximate any Poisson process in  $(0, T]$ . Similar to the analysis of Equation 4, we have an equivalent solution:

$$\sum_{i=1}^N \exp\left(\rho_i + \rho_o - \lambda_0 + \lambda^* + K \ln \frac{\lambda_0}{\lambda_1}\right) = 1, \quad (7)$$

where  $\rho_i$  and  $\rho_o$  denote the eigenvalue related to  $i$ -th spiking neuron and output neuron, respectively. It is worth noting that here  $\rho_o = \gamma/\tau$ , since there is only one output neuron (without adjacent neurons). Obviously, with flexible eigenvalues, Equation 7 has nontrivial solutions with  $N - 1$  degree of freedom. Further, we can declare that BSNN has nontrivial solutions for achieving the adaptive firing rate.

**Theorem 1** *If the bifurcation hyper-parameters  $\lambda_{ij}$  are all great than 0, there are at most  $2^{N-1}$  bifurcation solutions in Equation 6.*

**Proof:** The logic flow of Theorem 1 can be roughly proved by the following steps. First, finding the characteristic roots of our proposed BSNN model. According to Equation 6, we can obtain its algebraic representation as follows:

$$\tau \frac{d\mathbf{u}}{dt} = L_{\lambda} \mathbf{u} + G(\mathbf{u}, \lambda),$$

where

$$L_{\lambda} = A + B_{\lambda}, \quad G(\mathbf{u}, \lambda) = o(|\mathbf{u}|)$$

and

$$A = \begin{pmatrix} \gamma & & & \\ & \ddots & & \\ & & \ddots & \\ & & & \gamma \end{pmatrix}, \quad B_{\lambda} = \begin{pmatrix} 0 & \lambda_{12} & \cdots & \lambda_{1n} \\ \lambda_{21} & 0 & \cdots & \lambda_{2n} \\ \vdots & \vdots & \ddots & \vdots \\ \lambda_{n1} & \lambda_{n(n-1)} & \cdots & 0 \end{pmatrix}.$$

Suppose that the eigenvalues of the matrix  $B_{\lambda}$  are  $\beta_1, \dots, \beta_n$ . So the eigenvalue  $\rho_i$  of  $L_{\lambda}$  can be

represented as the sum of that of  $A$  and that of  $B_\lambda$ , that is,

$$\rho_i = \frac{-\gamma + \beta_i}{\tau}.$$

Next, we can elucidate the bifurcation solutions with respect to the eigenvalues. For simplicity, we take the 2-neuron model as an example, that is,

$$A = \begin{pmatrix} \gamma & 0 \\ 0 & \gamma \end{pmatrix}, \quad B_\lambda = \begin{pmatrix} 0 & \lambda_1 \\ \lambda_2 & 0 \end{pmatrix}.$$

Let

$$\begin{cases} D_1 = 2\gamma, \\ D_2 = \gamma^2 - \lambda_1\lambda_2, \end{cases}$$

then when  $\Delta = D_1^2 - 4D_2 = \lambda_1\lambda_2 \geq 0$ ,  $L_\lambda$  has two real eigenvalues:

$$\rho_1 = \frac{-D_1 - \sqrt{D_1^2 - 4D_2}}{2\tau},$$

and

$$\rho_2 = \frac{-D_1 + \sqrt{D_1^2 - 4D_2}}{2\tau}.$$

Obviously,  $\rho_1$  must be less than zero, but it is not necessary for  $\rho_2$ . Let  $\lambda_c = \gamma^2$  be the critical threshold, then the bifurcation solutions of Equation 6 are dominated by one pair of bifurcation eigenvalues:

$$\rho_1 = \frac{-D_1 - \sqrt{D_1^2 - 4D_2}}{2\tau} < 0,$$

$$\rho_2 = \frac{-D_1 + \sqrt{D_1^2 - 4D_2}}{2\tau} \begin{cases} < 0, & \lambda_1\lambda_2 < \lambda_c; \\ = 0, & \lambda_1\lambda_2 = \lambda_c; \\ > 0, & \lambda_1\lambda_2 > \lambda_c. \end{cases}$$

Merging  $\rho_1$  and  $\rho_2$  into Equation 7, we have:

$$\exp\left(\rho_1 + \frac{\gamma}{\tau} - \lambda_0 + \lambda^* + K \ln \frac{\lambda_0}{\lambda_1}\right) + \exp\left(\rho_2 + \frac{\gamma}{\tau} - \lambda_0 + \lambda^* + K \ln \frac{\lambda_0}{\lambda^*}\right) = 1.$$

Then the solution of Equation 7 becomes:

$$\exp\left(-\frac{\sqrt{\lambda_1\lambda_2}}{2\tau} - \lambda_0 + \lambda^* + K \ln \frac{\lambda_0}{\lambda^*}\right) + \exp\left(\frac{\sqrt{\lambda_1\lambda_2}}{2\tau}\right) = 1.$$

So as long as the product of  $\lambda_1$  and  $\lambda_2$  is greater than 0, there exists a least one nontrivial solutions of Equation 7 in BSNN. So the existence of bifurcation solutions is equivalent to the existence of nontrivial solutions of Equation 7; one pair of bifurcation solutions induces a group of apposite eigenvalues for achieving adaptive firing rates. Especially, when  $\lambda_1\lambda_2 < \lambda_c$ , both neurons work in a “leaky” mode; weaker signals would hinder neuron excitation. While  $\lambda_1\lambda_2 > \lambda_c$ , a new bifurcation phenomenon occurs, one neuron still works in a “leaky” mode, filtering weaker signals, but the other neuron appears to be active frequently. Generally, for the case of  $N$  neurons, the solution of Equation 6 possesses at most  $2^{N-1}$  bifurcation solutions.  $\square$

On the basis of the results of Theorem 1, the eigenvalues of Equation 6 are dominated by a series of bifurcation hyper-parameters  $\lambda$ . So we can convert the issue of achieving adaptive firing rates into the problem of how to calculate the bifurcation hyper-parameters  $\lambda$ . The learning procedure will be implemented in the next section.

### 4.3. Implementation

Consider a feed-forward BSNN with  $M$  pre-synaptic input channels and  $N$ -dimensional spiking neurons, and approximate the mutual promotion from the  $i$ -th neuron to the  $k$ -th neuron is caused by the last spike of neuron  $i$ , noted as  $u_i(\hat{t}_i)$ , where  $\hat{t}_i = \max\{t_i | t_i^{firing} \leq t\}$ . Then, for the  $k$ -th neuron, we have

$$\tau \frac{du_k(t)}{dt} = \gamma u_k(t) + \sum_{i=1, i \neq k}^N \lambda_{ki} u_i(\hat{t}_i) + \sum_{j=1}^M W_{kj} \cdot I_j(t). \quad (8)$$

In Equation 8, the bifurcation hyper-parameters are independent to connection weights, thus avoiding the problem of parameter entanglement.

Akin to the Spike Response Model (SRM) [Ger95], Equation 8 has a closed-form solution:

$$u_k(t) = \int_{t'}^t \exp\left(\gamma \frac{(s-t')}{\tau}\right) \cdot Q_k(s) ds, \quad (9)$$

where

$$Q_k(t) = \sum_{i \neq k} \lambda_{ki} u_i(\hat{t}_i) + \sum_{j=1}^M W_{kj} \cdot I_j(t). \quad (10)$$

By employing the spike excitation function  $f_e$ , the bifurcation spiking neurons can generate spikes to next neuron.

### Error Backpropagation in BSNN

BSNN with supervised signals can also be optimized via error backpropagation. Firstly, we denote the input spike train to a neuron as the following general form [HS18]:

$$I_j(t) = \sum_{firing} \epsilon_j \left( t - t_j^{firing} \right),$$

where  $t_j^{firing}$  is the spike time of the  $j$ -th input and  $\epsilon(t)$  is a corresponding Dirac-delta function.

Then summing up the loss of the  $k$ -th target supervised signal  $\hat{S}_k(t)$  related to  $S_k(t)$  in time interval  $[0, T]$ :

$$E_k = \frac{1}{2} \int_0^T E_k(t) dt = \frac{1}{2} \int_0^T \left( S_k(t) - \hat{S}_k(t) \right)^2 dt. \quad (11)$$

So for time  $t$ , we have

$$\frac{\partial E_k(t)}{\partial W_{kj}} = \frac{\partial E_k(t)}{\partial S_k} \frac{\partial S_k}{\partial u_k} \frac{\partial u_k}{\partial W_{kj}}. \quad (12)$$

As shown in Figure 2, the first term of Equation 12 represents the error backpropagation of the excitatory neurons, while the third term is the backpropagation of basic bifurcation neuron error. Plugging Equation 9 and Equation 11 into Equation 12, the gradient term can be calculated as:

$$\frac{\partial E_k(t)}{\partial W_{kj}} = \left( S_k(t) - \hat{S}_k(t) \right) f'_e(u_k) \delta_j(t),$$

where

$$\delta_j(t) = \frac{\epsilon_j(t)}{\tau} \exp\left(-\frac{\gamma t}{\tau}\right).$$

However, the derivative of the spike excitation function  $f'_e(u)$  is always a problem for training SNNs with

supervised signals. Recently, there have emerged many seminal approaches for addressing this problem. In this paper, we directly employ the result of [SO18].

Therefore, we obtain the backpropagation pipeline related to connection weights  $W_{kj}$ :

$$\nabla_{W_{kj}} E = \int_0^T \frac{\partial E_k(t)}{\partial W_{kj}} dt.$$

Similar to the error-backpropagation process with respect to  $W_{kj}$ , the correction formula with respect to  $\lambda_{ki}$  is given by:

$$\nabla_{\lambda_{ki}} E = \int_0^T \left( S_k(t) - \hat{S}_k(t) \right) f'_e(u_k) \frac{u_i(\hat{t}_i)}{\tau} \exp\left(-\frac{\gamma t}{\tau}\right) dt.$$

In general, we can also add a learning rate  $\eta$  to help convergence, just like most deep artificial neural networks.

Here, BSNN is implemented by an extended BP algorithm. Compared with the existing SNNs, BSNN only needs to calculate one more set of gradients, i.e.,  $\nabla_{\lambda_{ki}} E$  during feedback. The records of  $u_i(\hat{t}_i)$  do not cause additional storage, because we intrinsically need the membrane potential values of each spiking neuron during the gradient calculation procedure as shown in Equation 12. So both the computation and storage of BSNN are considerably less in comparison with the alternating optimization approaches.

## 5. Experiments

In this section, we conducted experiments on several tasks to evaluate the functional performance of BSNN.

The experiments are performed to discuss the following questions:

Q1: Is the performance of BSNN comparable with state-of-the-art SNNs?

Q2: Does the performance of BSNN surpass that of alternating optimization, especially in terms of accuracy and efficiency?

Q3: Concerning BSNN, is the performance robust to the control rate? In which conditions?

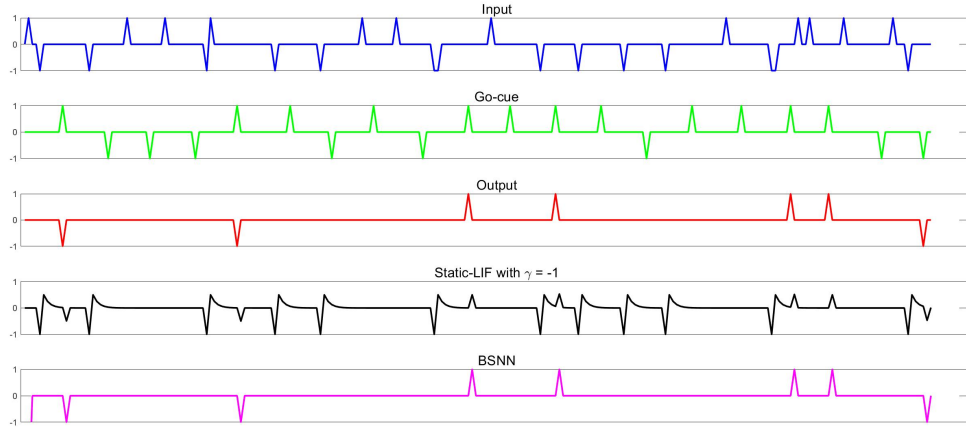


Figure 3: Delayed-memory XOR task. The panels from top to bottom are the single-trial input, go-cue signals, output traces, the prediction signals of the static-LIF SNN, and the prediction results of BSNN, respectively.

### 5.1. Delayed-memory XOR Task

We first consider a *Delayed-memory XOR* task, which performs the XOR operation on the input history stored over an extended duration [ADM16]. Specifically, the network receives two binary pulse signals, + or -, through an input channel and a go-cue channel. When the network receives two input pulses between two go-cue pulses, it should output the XOR signal of both inputs. In other words, the network outputs a positive signal if the input pulses are of equal signs (+ + or - -), and a negative signal if the input pulses are of opposite signs (+ - or - +). If there is only one input pulse between two go-cue pulses, the network should generate a null output.

Based on the above introduction, we simulated a Delayer-memory XOR dataset, which consists of 2400 input signals with 300 pulses, 2400 go-cue signals with 200 pulses, and the corresponding output signals. We also train the networks with the rest voltage  $u_{rest} = 0$  by the first 2160 units and predict the output signals of the last 240 signals.

Figure 3 displays the performance of the traditional SNN model with fixed control rate  $\gamma = -1$  (i.e., static-LIF SNN) and BSNN on delayed-memory XOR task, in which BSNN can be highly qualified with the correct outputs, whereas the static-LIF SNN frequently makes mistakes because it cannot distinguish the roles of different channel signals. These comparative results confirm that our proposed BSNN can perform nonlinear computations over an extended time.

## 5.2. Benchmark Tasks

We also test the performance of BSNN on 3 benchmark datasets. Limited by the space, we here only provide the core information of datasets, pre-processing, and the contenders. Detailed introduction of this benchmark experiment are offered in Appendix.

**Datasets:** (1) The MNIST handwritten digit dataset<sup>1</sup> comprises a training set of 60,000 examples and a test set of 10,000 examples in 10 classes, and each example is centered in a  $28 \times 28$  image. Using Poisson encoding, we produce a list of spike signals with a formation of  $784 \times T$  binary matrices, where  $T$  denotes the encoding length and each row represents a spike train at each pixel. (2) The Neuromorphic-MNIST (N-MNIST) dataset<sup>2</sup> is a spiking version of the original frame-based MNIST dataset. Each example in N-MNIST was converted into a form of spike trains by mounting the ATIS sensor on a motorized pan-tilt unit and having the sensor move while it views MNIST examples on an LCD monitor. It consists of the same 60,000 training and 10,000 testing samples as the original MNIST dataset, and is captured at the same visual scale as the original MNIST dataset ( $28 \times 28$  pixels) with both “on” and “off” spikes. (3) The Fashion-MNIST dataset<sup>3</sup> consists of a training set of 60,000 examples and a test set of 10,000 examples. And each example is a  $28 \times 28$  grayscale image, associated with a label from 10 classes.

**Pre-processing:** The pre-processing steps for are the same as the ones in [PPU<sup>+</sup>05, ANDL18], that is, each static image of (1) MNIST and (3) Fashion-MNIST is converted into a spike train using Poisson Encoding, while each example in N-MNIST was encoded by a Dynamic Audio / Vision Sensor (DAS / DVS).

**Contenders:** We also employ 2 types of contenders to competing with the proposed BSNN: (1) several state-of-the-art SNNs with SRM structure and (2) alternating optimization algorithms as shown in Section 3. In this work, all SNN models are without any convolution term. And the alternating optimization algorithms pre-sample a group of control rates from two uniform distributions, that is,  $U_1 = \mathcal{U}[-1, 0]$  and  $U_2 = \mathcal{U}[-1, 1]$ . For these image classification tasks, we set 5 output spiking neurons, which are corresponding to the classification labels. And the output label of SNNs is the one with the greatest spike count.

The experimental results are shown in Table 1 that lists the comparative performance (accuracy) and configurations (setting and epoch) of the contenders and BSNN on 3 digit datasets. As we can see, BSNN

---

<sup>1</sup><http://yann.lecun.com/exdb/mnist/>

<sup>2</sup><https://www.garrickorcharde.com/datasets/n-mnist>

<sup>3</sup><https://www.kaggle.com/zalando-research/fashionmnist>



Table 1: The comparative performance of the contenders and BSNN.

Datasets	Contenders	Accuracy (%)	Setting	Control Rate ( $\gamma$ )	Epochs
MNIST	Deep SNN [OW16]	97.80	28×28-300-300-10 ♠	-	50
	Deep SNN-BP [LDP16]	98.71	28×28-800-10	-	200
	SNN-EP ♡	97.63	28×28-500-10	-	25
	HM2-BP [JZL18]	98.84 ± 0.02	28×28-800-10	-	100
	SLAYER [SO18]	98.39 ± 0.04	28×28-500-500-10	-	50
	SLAYER- $U_1$ ♣	98.53 ± 0.03	28×28-500-500-10	-	-
	SLAYER- $U_2$	98.59 ± 0.01	28×28-500-500-10	-	-
	BSNN (this work)	<b>99.02 ± 0.04</b>	28×28-500-500-10	-0.21	50
NMNIST	SKIM [COL <sup>+</sup> 16]	92.87	2*28×28-10000-10	-	-
	Deep SNN-BP	98.78	2*28×28-800-10	-	200
	HM2-BP	98.84 ± 0.02	2*28×28-800-10	-	60
	SLAYER	98.89 ± 0.06	2*28×28-500-500-10	-	50
	SLAYER- $U_1$	99.01 ± 0.01	2*28×28-500-500-10	-	-
	SLAYER- $U_2$	99.07 ± 0.02	2*28×28-500-500-10	-	-
	BSNN (this work)	<b>99.24 ± 0.12</b>	2*28×28-500-500-10	-0.49	50
Fashion-MNIST	HM2-BP	88.99	28×28-400-400-10	-	15
	SLAYER	88.61 ± 0.17	28×28-500-500-10	-	50
	SLAYER- $U_1$	90.53 ± 0.04	28×28-500-500-10	-	-
	SLAYER- $U_2$	90.61 ± 0.02	28×28-500-500-10	-	-
	ST-RSBP [ZL19]	90.00 ± 0.13	28×28-400-R400-10 ◇	-	30
	BSNN (this work)	<b>91.22 ± 0.06</b>	28×28-500-500-10	-0.32	50

♠ : -300-300- denotes two hidden layers with 300 spiking neurons, while -800- is one hidden layer with 800 spiking neurons.

♡ : SNN-EP [OGW19] proposes an implementation for training SNN with equilibrium propagation.

♣ : - $U_1$  and - $U_2$  indicate the alternating optimization algorithms with parametric control rates sampled from  $U_1$  and  $U_2$ , respectively.

◇ : R400 represents a recurrent layer of 400 spiking neurons.

performs best against other competing approaches, achieving very superior testing accuracy (i.e., more than 99% on MNIST, around 99.24% on NMNIST, and more than 91% on Fashion-MNIST). It is a laudable result for SNNs. In addition, the approaches based on alternating optimization algorithms, such as SLAYER- $U_1$  and SLAYER- $U_2$ , steadily surpass the existing SNNs without learnable control rates, which demonstrates the way of parameterizing eigenvalues of spike generation functions is significant and effective to SNNs.

Figure 3 illustrates the spike raster plots of SLAYER, SLAYER- $U_2$ , and BSNN on the 4881-th MNIST testing sample with label 0, showing the firing rates and neuron excitation snapshots of these 3 approaches in detail. Correspondingly, we firstly convert this image into a spike train using Poisson Encoding, and then mark the classification label according to the greatest spike count in Layer Output. The spike raster plots of spiking neurons (in Layer 1, Layer 2, and Layer Output) of SLAYER, SLAYER- $U_2$ , and BSNN

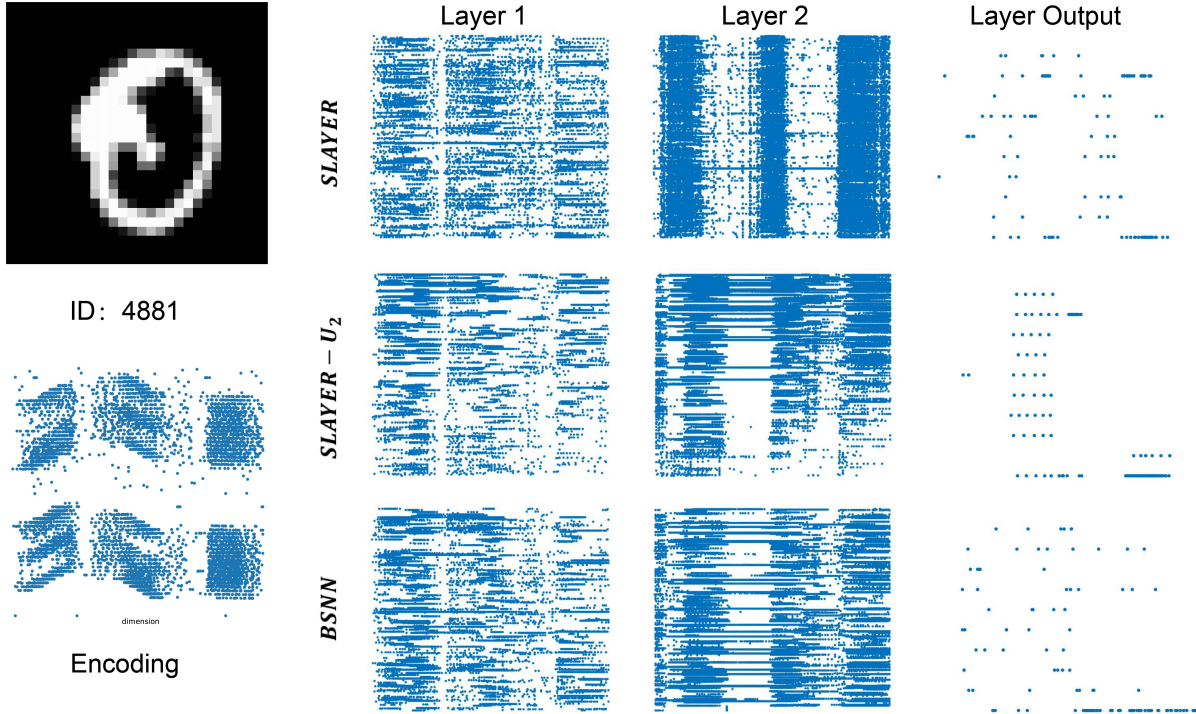


Figure 4: The spike raster plots of SLAYER, SLAYER- $U_2$ , and BSNN.

are successively shown in right 9 subplots. In SLAYER, the firing rate of spike neurons in the same layer is almost equal, so the output spikes are evenly generated, which causes the sample to be incorrectly classified as label 8. In contrast, both SLAYER- $U_2$  and BSNN are able to adaptively generate spikes. The firing rates of spiking neurons show significant differences; the output spiking neurons relative to wrong labels are suppressed, while the neuron relative to correct label is “encouraged” to fire spikes and eventually won out with a big advantage.

We also demonstrate the robustness of BSNN to the control rate. This experiment is conducted on the MNIST dataset, setting the architecture of BSNN as  $28 \times 28$ -500-500-10. For each control rate value, we ran BSNN 5 times, recorded the largest accuracy of each round within 50 epochs, and averaged 5 accuracy records as the testing performance. The results are plotted in Figure 5. Obviously, BSNN is able to perform better than the alternating optimization algorithms in a board-range setting of control rates.

Based on the aforementioned experiments and analysis, we can declare that BSNN achieves the superior performance to the existing SNNs and the improved contenders - the approaches based on alternating optimization algorithms. Additionally, the performance of BSNN is no longer sensitive to the setting of control rates.

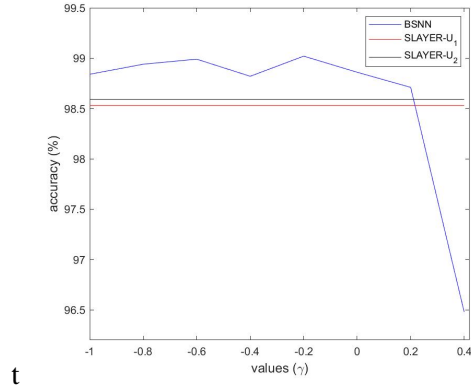


Figure 5: Robustness testing of BSNN with respect to control rates.

## 6. Conclusion and Discussions

In this paper, we attempt to achieve an adaptive firing rate in SNNs. We set out to address this issue with the eigenvalues of spike generation functions and reveal the close-knit relation between the two. Further, by employing the bifurcation theory to enable adaptable eigenvalues, we proposed the *Bifurcation Spiking Neural Network* (BSNN). Compared with the alternating optimization approaches, BSNN not only tackles the challenge that control rates interact with connection weights in training procedure, leading to a robust setting of control rates, but also works with a considerable less computation and storage. Finally, we demonstrate our model on a delayed-memory XOR task and 3 benchmark datasets. The experiments verify the effectiveness of BSNN.

We provided a series of theoretical discussions about the firing rates of spiking neurons and the bifurcation properties of BSNN, including and not limited to the relation between the firing rates and the eigenvalues of spike generation function, the algebraic structure of spike generation functions, and how to calculate the gradient for training BSNN. These results may promote the development of SNN-related theories. Besides, we also declare that our work doesn't aim at realizing a biological learning phenomenon but attempting to explore some new thoughts on SNNs. In this situation, Equation 8 that employs the last spikes of adjacent neurons to approximate the mutual promotion only provides a feasible paradigm of implementing dynamic bifurcation neurons. We are interested in scaling up our work.

## References

- [ADM16] Larry F Abbott, Brian DePasquale, and Raoul-Martin Memmesheimer. Building functional networks of spiking model neurons. *Nature Neuroscience*, 19(3):350, 2016.
- [ANDL18] Jithendar Anumula, Daniel Neil, Tobi Delbruck, and Shih-Chii Liu. Feature representations for neuromorphic audio spike streams. *Frontiers in Neuroscience*, 12:23, 2018.
- [BDM13] David G Barrett, Sophie Denève, and Christian K Machens. Firing rate predictions in optimal balanced networks. In *Advances in Neural Information Processing Systems 26 (NIPS)*, pages 1538–1546, 2013.
- [CCL19] Chi-Ning Chou, Kai-Min Chung, and Chi-Jen Lu. On the algorithmic power of spiking neural networks. In *Proceedings of the 10th Innovations in Theoretical Computer Science (ITCS)*, volume 26, pages 1–20, 2019.
- [COL<sup>+</sup>16] Gregory K Cohen, Garrick Orchard, Sio-Hoi Leng, Jonathan Tapson, Ryad B Benosman, and André Van Schaik. Skimming digits: Neuromorphic classification of spike-encoded images. *Frontiers in Neuroscience*, 10:184, 2016.
- [Ger95] Wulfram Gerstner. Time structure of the activity in neural network models. *Physical Review E*, 51(1):738, 1995.
- [GK02] Wulfram Gerstner and Werner M Kistler. *Spiking Neuron Models: Single Neurons, Populations, Plasticity*. Cambridge University Press, 2002.
- [HE15] Eric Hunsberger and Chris Eliasmith. Spiking deep networks with LIF neurons. *arXiv:1510.08829*, 2015.
- [HS18] Dongsung Huh and Terrence J Sejnowski. Gradient descent for spiking neural networks. In *Advances in Neural Information Processing Systems 31 (NIPS)*, pages 1440–1450, 2018.
- [JZL18] Yingyezhe Jin, Wenrui Zhang, and Peng Li. Hybrid macro/micro level backpropagation for training deep spiking neural networks. In *Advances in Neural Information Processing Systems 31 (NIPS)*, pages 7005–7015, 2018.
- [Kuz13] Yuri A Kuznetsov. *Elements of Applied Bifurcation Theory*. Springer, 2013.

- [LDP16] Jun Haeng Lee, Tobi Delbruck, and Michael Pfeiffer. Training deep spiking neural networks using backpropagation. *Frontiers in Neuroscience*, 10:508, 2016.
- [OGW19] Peter OConnor, Efstratios Gavves, and Max Welling. Training a spiking neural network with equilibrium propagation. In *Proceedings of the 22nd International Conference on Artificial Intelligence and Statistics (AISTATS)*, pages 1516–1523, 2019.
- [Onu02] Akira Onuki. *Phase Transition Dynamics*. Cambridge University Press, 2002.
- [OW16] Peter O’Connor and Max Welling. Deep spiking networks. *arXiv:1602.08323*, 2016.
- [PPU<sup>+</sup>05] Jonathan W Pillow, Liam Paninski, Valerie J Uzzell, Eero P Simoncelli, and EJ Chichilnisky. Prediction and decoding of retinal ganglion cell responses with a probabilistic spiking model. *Journal of Neuroscience*, 25(47):11003–11013, 2005.
- [QRK<sup>+</sup>05] R Quian Quiroga, Leila Reddy, Gabriel Kreiman, Christof Koch, and Itzhak Fried. Invariant visual representation by single neurons in the human brain. *Nature*, 435(7045):1102, 2005.
- [SO18] Sumit Bam Shrestha and Garrick Orchard. SLAYER: Spike layer error reassignment in time. In *Advances in Neural Information Processing Systems 31 (NIPS)*, pages 1419–1428, 2018.
- [VGT05] Rufin VanRullen, Rudy Guyonneau, and Simon J Thorpe. Spike times make sense. *Trends in Neurosciences*, 28(1):1–4, 2005.
- [ZL19] Wenrui Zhang and Peng Li. Spike-train level backpropagation for training deep recurrent spiking neural networks. In *Advances in Neural Information Processing Systems 32 (NeurIPS)*, pages 7800–7811, 2019.

## A. Eigenvalues and Algebraic Equations

For a system of first-order linear differential equations as follows:

$$\frac{d}{dt} \begin{pmatrix} u_1 \\ \vdots \\ u_n \end{pmatrix} = \begin{pmatrix} \alpha_{11} & \cdots & \alpha_{1n} \\ \vdots & \ddots & \vdots \\ \alpha_{n1} & \cdots & \alpha_{nn} \end{pmatrix} \cdot \begin{pmatrix} u_1 \\ \vdots \\ u_n \end{pmatrix} + \begin{pmatrix} f_1(t) \\ \vdots \\ f_n(t) \end{pmatrix},$$

we have its algebraic formulation:

$$\frac{d}{dt} \begin{pmatrix} \Delta_1 \\ \vdots \\ \Delta_n \end{pmatrix} = A \cdot \begin{pmatrix} \Delta_1 \\ \vdots \\ \Delta_n \end{pmatrix}, \quad \text{where } A = \begin{pmatrix} \alpha_{11} & \cdots & \alpha_{1n} \\ \vdots & \ddots & \vdots \\ \alpha_{n1} & \cdots & \alpha_{nn} \end{pmatrix}.$$

These algebraic equations are only related to the observation variables  $\Delta_1, \dots, \Delta_n$ . So the spectrum values (eigenvalues) of the matrix (operator)  $A$  lead to the evolution mechanism of this dynamic system.

## B. Bifurcation Structure in LIF Equation

We have done a lot of analysis in the text to illustrate the importance of the control rates to the performance of SNNs (that is, firing rates). In fact, the control rate intrinsically is a bifurcation hyper-parameter of the LIF model. In this appendix, we are going to interpret this conjecture. We start our analysis from a simplest form of the LIF model, which with input  $I(t)$  and a rest voltage  $u_{rest}$  is generally formulated as follows:

$$\tau \frac{du}{dt} = u_{rest} + \gamma \cdot u + R \cdot I(t), \tag{13}$$

where  $u(t)$  represents the membrane potential at time  $t$ ,  $\tau$  is the membrane time constant,  $\gamma$  is the control rate, usually preset to a fixed values  $-1$ , and  $R$  is the membrane resistance. This equation describes a resistor-capacitor circuit that the spiking neuron can only be activated when the membrane potential  $u(t)$  reaches a certain threshold  $u_{firing}$  (firing threshold). After firing, the neural membrane potential is instantaneously reset to a lower value  $u_{rest}$  (rest voltage).

Particularly, as a mathematical ODE model, the LIF equation has fixed eigenvalues  $\rho = \gamma$  by solving its algebraic formulation. This means the control rate in the LIF model is equal to its eigenvalue  $\rho$ .

Correspondingly, the LIF equation has a general solution as follows:

$$u(t) = \exp\left(\gamma \frac{(t-t')}{\tau}\right) \left[ u_{rest} + \frac{R}{\tau} \int_{t'}^t \exp\left(\gamma \frac{(t'-s)}{\tau}\right) I(s) ds \right],$$

where  $t'$  denotes the last firing time, that is,  $t' = \max\{s \mid u(s) = u_{firing}, s < t\}$ .

Consider a general case of constant input  $I(t) = I$  and generally assume  $u_{rest} = 0$ . The solution of Equation 13 can be converted into:

$$u(t) = \begin{cases} \frac{RI}{\gamma} \left[ \exp\left(\gamma \frac{(t-t')}{\tau}\right) - 1 \right], & \gamma \neq 0; \\ (t-t') \cdot I & , \gamma = 0. \end{cases}$$

Note that the next firing time  $t'' = \min\{s \mid u(s) = u_{firing}, s > t'\}$ , then the firing period is derived below:

$$\Delta T = t'' - t' = \begin{cases} \frac{\tau}{\gamma} \ln\left(\frac{u_{firing}\gamma + RI}{RI}\right), & \gamma \neq 0; \\ \frac{u_{firing}}{RI} & , \gamma = 0. \end{cases}$$

So the firing rate of the LIF neuron becomes:

$$f(\gamma, I) = \frac{1}{\Delta T} = \frac{\gamma}{\tau \ln\left(\frac{u_{firing}\gamma + RI}{RI}\right)}, \quad (14)$$

with the condition  $u_{firing}\gamma + RI > 0$ .

According to the formation of a two-variable function, there are obviously two core conclusions about  $f(\gamma, I)$ : (1)  $f(\gamma, I)$  is an increasing function with respect to  $\gamma$  and  $I$ , respectively; (2) the firing rate of a spiking neuron is sensitive to the control rate. In detail, the establishment condition  $u_{firing}\gamma + RI > 0$  causes an inactivated area in the domain, which is plotted in Figure 6(a). This means that for a pre-given negative  $\gamma$ , the signals weaker than  $u_{firing} |\gamma| / R$  are detrimental to activate a LIF neuron, such as the simulated case that  $I = 4$ ,  $\gamma = -0.5$ , and  $R = 1$  in Figure 6(b). Additionally,

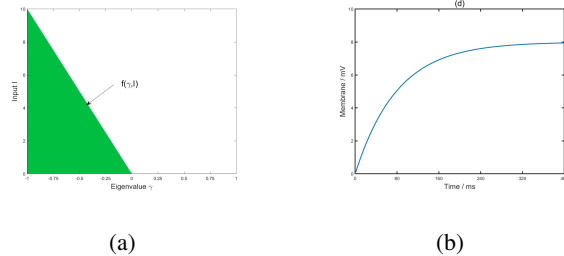


Figure 6: (a) Inactivated “dead zone” of the neuron excitation frequency function with  $u_{firing} = 10$  and  $R = 1$ . (b) The neuron with  $I = 4$ ,  $\gamma = -0.5$ , and  $R = 1$  is hard to be activated.

the inactivated area is dominated by the sign of  $\gamma$ ; when  $\gamma$  is greater than 0, the neuron can always be activated, no matter what input, whereas once  $\gamma$  becomes negative, there is inevitably a situation in which neurons cannot be activated, although the input signals in reality are evolving according to time.

In summary, control rates of the LIF neuron are indeed have a great and sensitive influence on the firing rate of spiking neurons; both the magnitude and sign of the eigenvalue will affect the generation frequency of the spikes. When the control rates pass through the critical points, the LIF model has a topological change.